

Propagation of uncertainties in the nuclear DFT models

Markus Kortelainen

Department of Physics, P.O. Box 35 (YFL), University of Jyväskylä, FI-40014
Jyväskylä, Finland

Helsinki Institute of Physics, P.O. Box 64, FI-00014 University of Helsinki, Finland

E-mail: markus.kortelainen@jyu.fi

Abstract. Parameters of the nuclear density functional theory (DFT) models are usually adjusted to experimental data. As a result they carry certain theoretical error, which, as a consequence, carries out to the predicted quantities. In this work we address the propagation of theoretical error, within the nuclear DFT models, from the model parameters to the predicted observables. In particular, the focus is set on the Skyrme energy density functional models.

PACS numbers: 21.10.-k, 21.30.Fe, 21.60.Jz

1. Introduction

The purpose of the theoretical models is not only to explain current observations, but also to make predictions to be tested with the future observations. In nuclear physics particularly, there still exists a wide gap between experimentally known nuclei and the expected limits of the nuclear landscape, in particular for the heavier, very neutron rich nuclei [1]. Even though these nuclei are yet to be observed in the laboratory, many of them have impact on astrophysical scenarios [2]. To predict properties of nuclei, various theoretical models have been developed and applied. In extrapolation to experimentally unknown region, the role of model uncertainties becomes prominent. Without accompanied error analysis, the model prediction bears no meaning.

Presently, the nuclear density functional theory (DFT) is the only microscopic theory which can be applied throughout the entire nuclear chart. The key ingredient of the DFT is the energy density functional (EDF), which incorporates complex many-body correlations into a functional, which is constructed from the nucleonic densities and currents. Currently, there are three main variants of the nuclear DFT; zero-range Skyrme, finite range Gogny, and relativistic mean field models [3]. In this work we focus on the Skyrme-EDF models. Similar kind of analysis for other nuclear DFT variants could be also done.

Similarly like with any other effective theory, the parameters of the nuclear DFT models need to be adjusted to empirical input. Historically, in the optimization of various nuclear DFT models, covariance error analysis of the obtained parameterization was usually neglected. However, as stressed for example in [4, 5], error analysis is an essential post-optimization tool to quantify the model errors. Only very recently, such kind of analysis has been performed for nuclear DFT models [6, 7, 8, 9, 10, 11]. This kind of information is vital when assessing predictive power of the model.

Theoretical uncertainties related to the limits of the nuclear landscape, within Skyrme-EDF models, were studied in [1]. It was found that, despite large differences in various optimization procedures, current Skyrme-EDF models give a rather consistent picture about the position of the proton and neutron drip-lines. Furthermore, it was found that both, systematic model error and statistical model error, gave rather similar uncertainty width for the drip-line. Similar studies for relativistic mean-field models were also done in [12, 13]. The results were rather similar to Skyrme-EDF results. Uncertainties within the Brussels-Montreal HFB mass models were analyzed in [14].

With a given covariance matrix of the model, the propagation of the error from the model parameters to the model predictions can be computed. The information content and effect of a new observable to the uncertainties of the model parameters and predictions was investigated in [15]. It was found that a precise measurement of neutron skin thickness in ^{208}Pb could reduce model errors of other isovector observables. In [16] propagation of the error within UNEDF0 EDF [7] model was investigated in semi-magic nuclei. Statistical and systematic model errors related to the neutron skin thickness were studied in [17]. In both of these studies, the poorly constrained isovector

parameters were found to be the largest source to the model error.

This article is organized as follows: In Section 2 we review theoretical formalism. Some examples are discussed in Section 3, and in Section 4 we present concluding remarks.

2. Theoretical framework

2.1. Skyrme energy density

In the Skyrme-EDF framework the total binding energy E of the nucleus is

$$E = \int d^3r (\mathcal{E}^{\text{Kin}}(\mathbf{r}) + \mathcal{E}_0^{\text{Sk}}(\mathbf{r}) + \mathcal{E}_1^{\text{Sk}}(\mathbf{r}) + \mathcal{E}^{\text{Pair}}(\mathbf{r}) + \mathcal{E}^{\text{Coul}}(\mathbf{r})) , \quad (1)$$

where $\mathcal{E}^{\text{Kin}}(\mathbf{r})$ is the kinetic energy density, $\mathcal{E}^{\text{Pair}}(\mathbf{r})$ is the pairing energy density, and $\mathcal{E}^{\text{Coul}}(\mathbf{r})$ is the Coulomb energy density. Isoscalar ($t = 0$) and isovector ($t = 1$) time-even part of the Skyrme energy density is defined as

$$\mathcal{E}_t^{\text{Sk}}(\mathbf{r}) = C_t^\rho[\rho]\rho_t^2 + C_t^\tau\rho_t\tau_t + C_t^{\Delta\rho}\rho_t\Delta\rho_t + C_t^{\nabla J}\rho_t\nabla\cdot\mathbf{J}_t + C_t^J\mathbb{J}_t^2 , \quad (2)$$

where density dependency is

$$C_t^\rho[\rho] = C_{t0}^\rho + C_{tD}^\rho\rho_0^\gamma . \quad (3)$$

In equations above, we have omitted, for brevity, dependence of densities on the spatial coordinate \mathbf{r} . The Skyrme energy density (2) is composed of matter density ρ_t , kinetic density τ_t , spin-current vector density \mathbf{J}_t , and spin-current tensor density \mathbb{J}_t . Isoscalar matter density is defined as $\rho_0 = \rho_n + \rho_p$, and isovector matter density as $\rho_1 = \rho_n - \rho_p$, where n and p are neutron and proton indices, respectively. Isoscalar and isovector density is defined similarly also for the kinetic and spin-current densities. Standard definitions of these densities can be found e.g. in [3, 18]. Here, $C_t^\rho[\rho]\rho_t^2$ is the local volume term, which gives the largest contribution coming from the energy density to the total binding energy. Term $C_t^\tau\rho_t\tau_t$ is connected to the effective mass. Term $C_t^{\Delta\rho}\rho_t\Delta\rho_t$ is the local surface term, which mostly contributes at the surface of the nucleus. Furthermore, $C_t^{\nabla J}\rho_t\nabla\cdot\mathbf{J}_t$ and $C_t^J\mathbb{J}_t^2$ are the spin-orbit and tensor terms, respectively. The effect of spin-orbit term (and tensor term to lesser extend) is to push spin-orbit partner orbitals apart, to reproduce correct magic numbers.

The Skyrme energy density of equation (2) is parameterized by the coupling constants C_t^i . At the present, these parameters can not be pre-calculated from any theory within sufficient accuracy and, therefore, they need to be adjusted to empirical input. There is also a one-to-one correspondence between Skyrme coupling constants of the volume part, that is $\{C_{t0}^\rho, C_{tD}^\rho, C_t^\tau, \gamma; t = 0, 1\}$, and infinite nuclear matter (INM) parameters [19, 7]. Corresponding INM parameters have been listed on Table 1. INM parameters present a more convenient way to parameterize a part of the EDF since their values are approximately known.

To solve the ground state wave-function, within the single-reference Skyrme-EDF framework, one has to solve the Hartree-Fock or Hartree-Fock-Bogoliubov equations self-consistently. This procedure is outlined, e.g., in [3, 20].

Table 1. Infinite nuclear matter parameters.

Symbol	Explanation
ρ_c	Equilibrium density of the nuclear-matter
E^{NM}/A	Total energy per nucleon at equilibrium
K^{NM}	Nuclear-matter incompressibility
m_s^*/m	Scalar effective mass
$a_{\text{sym}}^{\text{NM}}$	Symmetry energy coefficient
$L_{\text{sym}}^{\text{NM}}$	Density dependence of the symmetry energy
m_v^*/m	Vector effective mass

2.2. Optimization of the model parameters

With the DFT models used in nuclear theory, the model parameters are usually adjusted to empirical input, and in some occasions, to some other pseudo-data not directly related to experimental result. Typical adjustment involves a minimization of the χ^2 function, which is usually defined as

$$\chi^2(\mathbf{x}) = \sum_{i=1}^{n_d} \left(\frac{s_i(\mathbf{x}) - d_i}{w_i} \right)^2, \quad (4)$$

where \mathbf{x} is an array of model parameters, $s_i(\mathbf{x})$ is the value of data point calculated from the model, and d_i is the corresponding empirical value for data point. Furthermore, n_d is the number of data points, and w_i is the used weight of the data point. The definition $\chi^2(\mathbf{x})$ is such that it is a unitless function. To obtain the minimum of the $\chi^2(\mathbf{x})$, at $\mathbf{x} = \mathbf{x}_{\text{min}}$, various algorithms can be used. In optimization of UNEDF energy density functionals POUNDERS algorithm was used, which offers significant improvement in terms of used CPU time compared to traditional Nelder-Mead algorithm [7].

As for the empirical input, nuclear DFT models have been typically optimized to various ground-state properties, see e.g. review in [3]. In optimization of UNEDF0 [7], binding energies, charge radii, and odd-even staggering data was used. For UNEDF1 [9] optimization, data on the fission isomer excitation energies were added to the pool of data points. As a result, fission properties were significantly improved. With UNEDF2 [11], shell structure was addressed by including data on single-particle level energies.

2.3. Determination of covariance matrix

The calculated model predictions $s_i(\mathbf{x})$ of equation (4) are, in nuclear DFT models, usually non-linear functions with respect of model parameters \mathbf{x} . In this kind of situation, a rigorous calculation of the covariance matrix is a formidable task, yet to be done. Therefore, usually a linearized least square system in the vicinity of the minimum \mathbf{x}_{min} of the object $\chi^2(\mathbf{x})$ function is assumed. Within this approximation, the $s_i(\mathbf{x})$ is assumed to be a linear function of \mathbf{x} . The validity of this approximation depends on the type of the observable and investigated width of the landscape around the minimum. For example, single-particle energies behave rather linearly with respect

of Skyrme coupling constants [21, 22]. Also, since the total energy E in the Skyrme-EDF scheme is directly proportional to the coupling constants, as shown in equation (2), it should also behave relatively linearly. This apparent linearity was also used in [23, 24] for parameter optimization. Nevertheless, non-linearities appear in self-consistent picture, where calculated densities depend on the coupling constants. A linearized approximation to covariance matrix is also numerically more stable compared to alternative choices [7].

Within aforementioned linearized approximation, covariance matrix of the model can be written as a matrix equation [5, 25]

$$\text{Cov}(x_i, x_j) = \left[(A^T G_w A)^{-1} \right]_{ij}, \quad (5)$$

where

$$A_{ij} = \left. \frac{\partial s_i(\mathbf{x})}{\partial x_j} \right|_{\mathbf{x}=\mathbf{x}_{\min}}, \quad (6)$$

$$G_w = \text{diag}(w_1^{-2}, \dots, w_{n_d}^{-2}), \quad (7)$$

where the weights w_i are the same weights as used in the $\chi^2(\mathbf{x})$ of equation (4). Derivatives of equation (6) typically need to be calculated numerically e.g. by taking a finite difference. However, in some cases a closed analytic form may be available. The normalization of $\chi^2(\mathbf{x})$ of equation (4) and covariance matrix (5) is selected according to "simple" convention of [5]. See the Appendix of [5] for other conventions.

Closely connected to the covariance matrix is the correlation coefficient between two model parameters, which is defined as

$$R_{ij} = \frac{\text{Cov}(x_i, x_j)}{\sqrt{\text{Var}(x_i)\text{Var}(x_j)}}, \quad (8)$$

where $\text{Var}(x_i) = \sigma_i^2$, and σ_i is the standard deviation of model parameter x_i . A strong correlation coefficient between two model parameters indicates that the covariance ellipsoid of the $\chi^2(\mathbf{x})$ landscape, close to the minimum, is strongly elongated [15].

As an example, figure 1 shows the correlation matrix of UNEDF0 parameterization [7]. From the figure, one can see that some of the volume parameters are strongly correlated with each other, as well as with the isoscalar surface coupling constant $C_0^{\rho\Delta\rho}$.

2.4. Propagation of error

With the covariance matrix known, the standard deviation $\sigma(O)$ of an observable O can be calculated as

$$\sigma^2(O) = \sum_{i,j} \text{Cov}(x_i, x_j) \left(\frac{\partial O(\mathbf{x})}{\partial x_i} \right) \left(\frac{\partial O(\mathbf{x})}{\partial x_j} \right) \Big|_{\mathbf{x}=\mathbf{x}_{\min}}, \quad (9)$$

where $O(\mathbf{x})$ is the predicted value of the observable by the model. Again, as with the calculation of the covariance matrix, derivatives with respect to model parameters usually need to be calculated numerically, by taking a finite difference. The standard deviation $\sigma(O)$ can be also referred, loosely speaking, as a "theoretical error". However, one should bear in mind, that there are also many other sources of theoretical errors, and it may be very difficult task to estimate the total combined theoretical error.

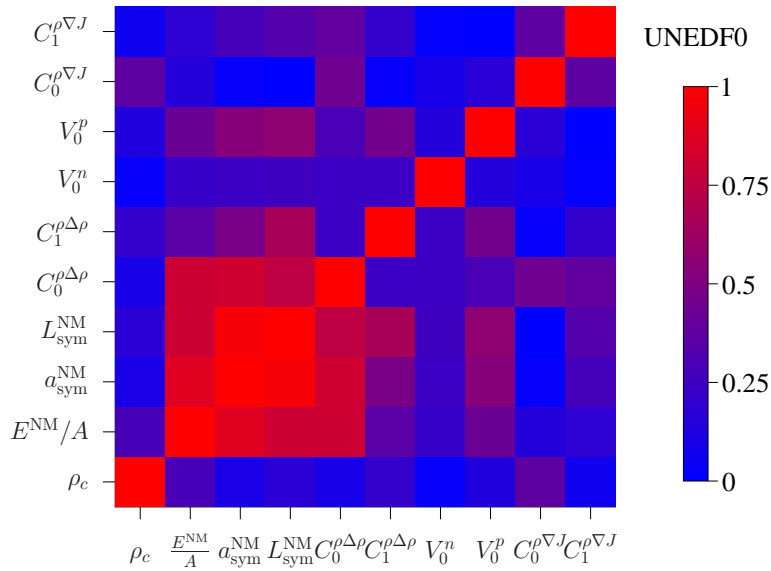


Figure 1. Correlation matrix of UNEDF0 parameterization presented graphically. Shown are absolute values of correlation coefficients.

2.5. Selection of weights

Up to so far, we have not defined what the weights w_i of equation (4) should be. The selection of the weights brings some arbitrariness to the adjustment of the model parameters. The position of the minimum \mathbf{x}_{min} depends on the relative magnitude of the used weights between various data points. By changing relative weighting between, e.g., binding energies and charge radii, the EDF model could be tailored to reproduce this kind of data more accurately. As a consequence, in the various EDF optimization schemes, there has not been a common practice regarding of selection of the weights.

To reduce this kind of arbitrariness, one option would be to use experimental error bars as a weights of the data points in equation (4). However, in the light of the performance of current EDF models, this is hardly a viable solution. Experimental mass measurements with Penning-traps can reach up to sub-keV level in accuracy [26], which is orders of magnitude more precise compared to expected accuracy of roughly 1 MeV of the present day mean-field models. With single particle (s.p.) energies, the situation is the same. Current Skyrme-like functionals can reproduce empirical s.p. data only with a typical root-mean-square (r.m.s.) deviation of roughly 1 MeV [21, 11, 22].

The other alternative is to tune the weights according to the capabilities of the used theoretical framework. As argued in [16], the weights should reflect expected accuracy of the model. Indeed, this has been the usual choice in many recent Skyrme-EDF optimization schemes. For example, in optimization of UNEDF0, the weights for nuclear binding energy data points were set to 2 MeV, and for the charge radii 0.02 fm. This corresponds rather well the overall performance on UNEDF0: The r.m.s. deviation for binding energies, over the whole even-even mass table, was 1.4 MeV and for the charge radii 0.017 fm. At the present, due to the lack of any better guideline, it seems that the

most appropriate way to set the weights is to use expected accuracy of the model for a each given data type.

3. Some examples

In this section, some illustrative examples about the propagation of theoretical error are shown. Examples are mainly calculated with UNEDF0 Skyrme-EDF. However, similar studies can be also done with other EDFs where the full covariance matrix of the model parameters is known.

3.1. Binding energies and separation energies

One of the most rudimentary observable, which a universal nuclear EDF is expected to reproduce well across the nuclear chart, is the binding energy. As discussed in Sec. 2.5, presently nuclear DFT models have a typical r.m.s. deviation from experimental data of the order of 1 MeV. Since the calculated total energy E , within the Skyrme-EDF model, is directly connected to the model parameters, the uncertainty of these parameters propagates to the predicted energy.

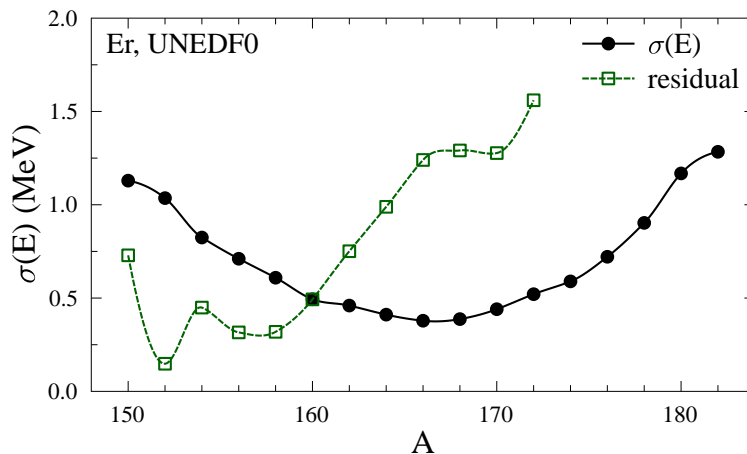


Figure 2. Calculated theoretical standard deviation $\sigma(E)$ of binding energies together with the absolute values of residuals to the experimental data in Er isotopic chain, with UNEDF0 EDF. All in units of MeV.

Figure 2 shows the calculated theoretical error in predicted binding energies of even-even erbium isotopes within UNEDF0 EDF model. Shown are also absolute values of residuals compared to experimental data of [27], that is, the difference between experimental and theoretical result. The results, as well as the results of Sec. 3.2, were calculated with computer code HFBTHO [28]. Since the volume part of UNEDF0 is parameterized with INM parameters, as well as corresponding part of the covariance matrix, they are also used here in calculation of derivatives of equation (9). Tensor coupling constants C_t^J in the UNEDF0 EDF model are set to zero. Propagation of error

to the binding energies of semi-magic isotopic and isotonic chains was also studied in [16]. Similarly as in [16], the propagated error here increases when moving further out from the valley of stability. Relation of the model residuals to experimental data was also investigated for lead isotopic chain, and it was found that around double-magic ^{208}Pb , the residuals were much larger compared to propagated error. This, and the fact that residuals along the isotopic chains are not randomly distributed, but usually show arc-like features (see e.g. [7]), are clear examples of the deficiency of the model. Here, in Er isotopic chain, the difference between residuals and propagated error is not as drastic, due to the fact that this kind of Skyrme EDF models are expected to perform better in deformed open shell nuclei.

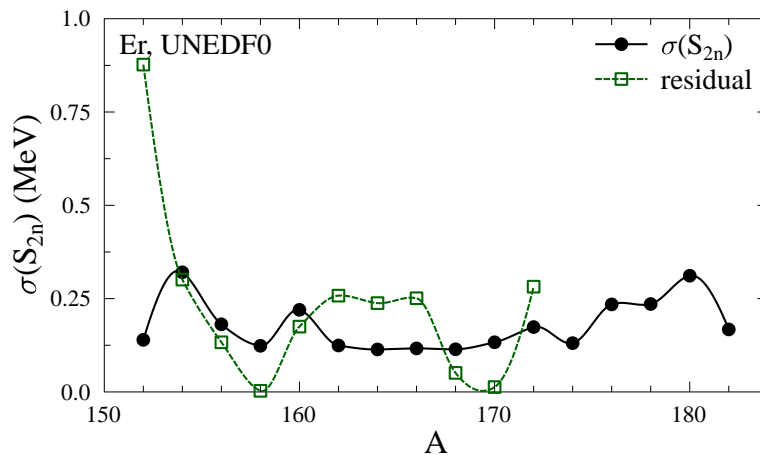


Figure 3. The same as figure 2, but for the two-neutron separation energies.

Theoretical error for two-neutrons separation energies is shown in figure 3 along with the residuals to experimental values for UNEDF0. As can be seen, the magnitude of residuals and the magnitude of theoretical error is usually rather similar. This is an indication that the weights selected for UNEDF0 optimization are in balance with expected accuracy of the model. The only notable deviation exists at the magic neutron number $N = 82$. Theoretical error for two-neutron separation energy was also studied in [1] for SV-min [6] EDF. Similarly as with SV-min, the error increases towards neutron rich regime. The same was also found in [16].

3.2. Neutron skin thickness

Recently, there has been a considerable theoretical and experimental interest on the neutron skin thickness. Neutron skin is defined as a neutron matter distribution extending further out compared to proton matter distribution. Neutron skin can be characterized by its thickness, which correlates strongly with other isovector observables [29, 30, 15, 31, 32, 33, 34, 35]. It has also a strong connection to neutron matter equation of the state [36, 37, 38, 39, 40, 10]. Experimentally, various probes have been used to determine neutron skin thickness. A recent measurement, the Lead Radius Experiment

(PREX) [41], determined the parity-violating asymmetry coefficient in ^{208}Pb , which is directly related to the neutron skin thickness providing $r_{\text{ns}} = 0.33^{+0.16}_{-0.18}$ fm [42]. This is probably the most model independent measurement of the neutron skin thickness.

Error propagation to predicted neutron skin thickness was studied in [17], where both, systematic and statistical, model error were addressed. One of the major outcomes of [17] was that the statistical model error is the defining theoretical uncertainty in the case of neutron skin thickness, whereas systematic model error was found to be notably lower.

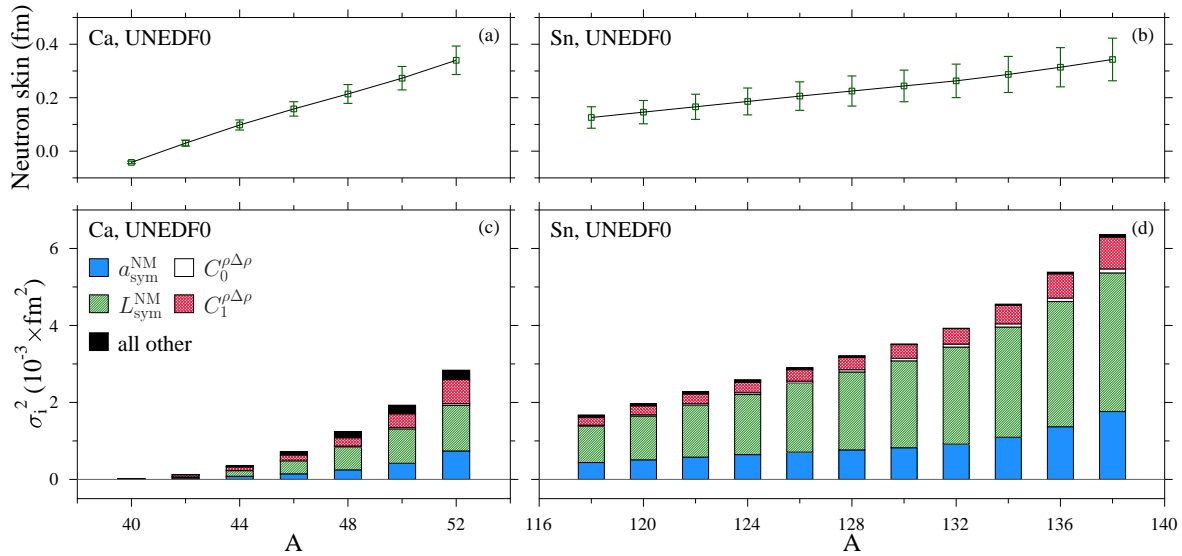


Figure 4. Upper panels: Predicted neutron skin thickness with theoretical uncertainty for Ca (a) and Sn (b) isotopic chains in units of fm. Lower panels: Theoretical error budget for neutron skin uncertainty for Ca (c) and Sn (d) isotopic chains. All calculated with UNEDF0 EDF.

Figure 4 shows predicted neutron skin thickness in even-even calcium and tin isotopes together with theoretical statistical error and error budget. Both, neutron skin thickness and related theoretical uncertainty, increase towards more neutron rich isotopes. As shown on the lower panels, the density dependence of the symmetry energy, $L_{\text{sym}}^{\text{NM}}$, has the largest contribution to the total error of the neutron skin thickness in both, calcium and tin isotopes. The situation was found to be the same also for lead isotopes in [17]. The second largest contributor comes from symmetry energy, $a_{\text{sym}}^{\text{NM}}$, similarly again as was found in [17]. This is one example, among many others, about the poorly determined isovector parameters in the EDF models.

Current status related to the uncertainties of the neutron skin thickness in ^{208}Pb is summarized in figure 5, which shows the result of PREX experiment together with systematic model error of [32], and the systematic and statistical model error obtained in [17]. The statistical model error is shown for UNEDF0 and SV-min EDFs. As discussed in [17] the PREX measurement, with a rather large error bar, can not constrain current EDF models. Planned PREX-II [43] and CREX [44] experiments, which will measure

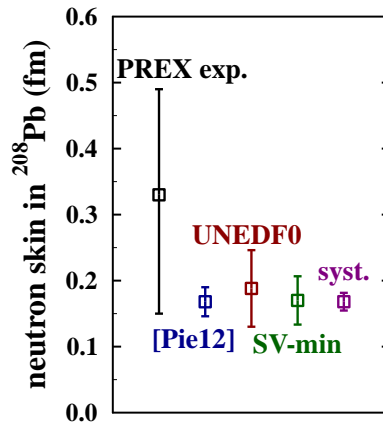


Figure 5. Experimental PREX result and theoretical model predictions with error bars for the neutron skin thickness in ^{208}Pb . Label [Pie12] refers to systematic model average of [32]. UNEDF0, SV-min and systematic model error are taken from [17]. All in units of fm.

neutron skin thickness in ^{208}Pb and ^{48}Ca , aim at much higher experimental accuracy. Results provided by these experiments could help to constrain isovector parameters in the future EDF optimization schemes.

4. Concluding remarks

In this article, we have analyzed theoretical uncertainties related to the nuclear EDF models. In particular, the focus has been on the propagation of the error to the predicted observables within the framework of UNEDF0 Skyrme EDF. Nuclear binding energies, two-neutron separation energies and neutron skin thickness were used as an examples. In all cases, as well as in the previous studies, it was found that theoretical error increases towards increasing isospin excess. This has been directly linked to the poorly known isovector parameters of the EDFs. Similar kind of analysis could be done for other EDF models, where information about the covariance matrix exists. Nevertheless, with this kind of analysis, one should always bear in mind, that the procedure outlined in this article can only assess theoretical uncertainties within the model itself. Uncertainties and model errors connected to the deficiency of the model itself can not be estimated with this procedure. One signature of such kind of deficiency is a clear pattern of residuals of experimental data, which are significantly larger compared to calculated theoretical model error. In [16] binding energies close to double-magic ^{208}Pb , and single-particle energies were found to follow this kind of pattern. Yet another source of errors are the used numerical and computational procedures.

In the future EDF parameter optimization schemes, sensitivity analysis of the obtained parameterization will be prime importance. Without such a procedure, there is no handle to judge the predictive power of the model. As concluded in [11], the limits of the Skyrme-like EDFs have been reached and major improvements are not to be expected on this path. To go beyond present day EDF models, many alternatives

have been presented [45, 24, 46]. Nonetheless, all of them share the common feature of the requirement to adjust the model parameters to empirical input. It will be exciting to see how these new EDF models perform across the nuclear chart and how good will be their predictive power.

Acknowledgments

This work was supported by the Academy of Finland under the Centre of Excellence Programme 2012-2017 (Nuclear and Accelerator Based Physics Programme at JYFL) and under the FIDIPRO programme, and by the European Unions Seventh Framework Programme ENSAR (THEXO) under Grant No. 262010. We acknowledge the CSC - IT Center for Science Ltd, Finland, for the allocation of computational resources.

References

- [1] J. Erler, N. Birge, M. Kortelainen, W. Nazarewicz, E. Olsen, A.M. Perhac, and M. Stoitsov. The limits of the nuclear landscape. *Nature*, 486:509, 2012.
- [2] A. Aprahamian, I. Bentley, M. Mumpower, and R. Surman. Sensitivity studies for the main r process: nuclear masses. *AIP Advances*, 4:041101, 2014.
- [3] M. Bender, P.-H. Heenen, and P.-G. Reinhard. Self-consistent mean-field models for nuclear structure. *Rev. Mod. Phys.*, 75:121, 2003.
- [4] J. Toivanen, J. Dobaczewski, M. Kortelainen, and K. Mizuyama. Error analysis of nuclear mass fits. *Phys. Rev. C*, 78:034306, 2008.
- [5] J Dobaczewski, W Nazarewicz, and P-G Reinhard. Error estimates of theoretical models: a guide. *J. Phys. G*, 41:074001, 2014.
- [6] P. Klüpfel, P.-G. Reinhard, T. J. Bürvenich, and J. A. Maruhn. Variations on a theme by skyrme: A systematic study of adjustments of model parameters. *Phys. Rev. C*, 79:034310, 2009.
- [7] M. Kortelainen, T. Lesinski, J. Moré, W. Nazarewicz, J. Sarich, N. Schunck, M. V. Stoitsov, and S. Wild. Nuclear energy density optimization. *Phys. Rev. C*, 82:024313, 2010.
- [8] F. J. Fattoyev and J. Piekarewicz. Accurate calibration of relativistic mean-field models: Correlating observables and providing meaningful theoretical uncertainties. *Phys. Rev. C*, 84:064302, 2011.
- [9] M. Kortelainen, J. McDonnell, W. Nazarewicz, P.-G. Reinhard, J. Sarich, N. Schunck, M. V. Stoitsov, and S. M. Wild. Nuclear energy density optimization: Large deformations. *Phys. Rev. C*, 85:024304, 2012.
- [10] J. Erler, C. J. Horowitz, W. Nazarewicz, M. Rafalski, and P.-G. Reinhard. Energy density functional for nuclei and neutron stars. *Phys. Rev. C*, 87:044320, 2013.
- [11] M. Kortelainen, J. McDonnell, W. Nazarewicz, E. Olsen, P.-G. Reinhard, J. Sarich, N. Schunck, S. M. Wild, D. Davesne, J. Erler, and A. Pastore. Nuclear energy density optimization: Shell structure. *Phys. Rev. C*, 89:054314, 2014.
- [12] A.V. Afanasjev, S.E. Agbemava, D. Ray, and P. Ring. Nuclear landscape in covariant density functional theory. *Phys. Lett. B*, 726:680, 2013.
- [13] S. E. Agbemava, A. V. Afanasjev, D. Ray, and P. Ring. Global performance of covariant energy density functionals: Ground state observables of even-even nuclei and the estimate of theoretical uncertainties. *Phys. Rev. C*, 89:054320, 2014.
- [14] S. Goriely and R. Capote. Uncertainties of mass extrapolations in hartree-fock-bogoliubov mass models. *Phys. Rev. C*, 89:054318, 2014.
- [15] P.-G. Reinhard and W. Nazarewicz. Information content of a new observable: The case of the nuclear neutron skin. *Phys. Rev. C*, 81:051303, 2010.

- [16] Y. Gao, J. Dobaczewski, M. Kortelainen, J. Toivanen, and D. Tarpanov. Propagation of uncertainties in the skyrme energy-density-functional model. *Phys. Rev. C*, 87:034324, 2013.
- [17] M. Kortelainen, J. Erler, W. Nazarewicz, N. Birge, Y. Gao, and E. Olsen. Neutron-skin uncertainties of skyrme energy density functionals. *Phys. Rev. C*, 88:031305, 2013.
- [18] J Dobaczewski and J Dudek. *Acta Phys. Pol. B*, 27:45, 1996.
- [19] B. K. Agrawal, S. Shlomo, and V. Kim Au. Determination of the parameters of a skyrme type effective interaction using the simulated annealing approach. *Phys. Rev. C*, 72:014310, 2005.
- [20] P. Ring and P. Schuck. *The Nuclear Many-Body Problem*. Springer, 2000.
- [21] M. Kortelainen, J. Dobaczewski, K. Mizuyama, and J. Toivanen. Dependence of single-particle energies on coupling constants of the nuclear energy density functional. *Phys. Rev. C*, 77:064307, 2008.
- [22] D. Tarpanov, J. Dobaczewski, J. Toivanen, and B.G. Carlsson. Spectroscopic properties of nuclear skyrme energy density functionals. *arXiv:1405.4823*, 2014.
- [23] G. F. Bertsch, B. Sabbey, and M. Uusnäkki. Fitting theories of nuclear binding energies. *Phys. Rev. C*, 71:054311, 2005.
- [24] M. Stoitsov, M. Kortelainen, S. K. Bogner, T. Duguet, R. J. Furnstahl, B. Gebremariam, and N. Schunck. Microscopically based energy density functionals for nuclei using the density matrix expansion: Implementation and pre-optimization. *Phys. Rev. C*, 82:054307, 2010.
- [25] S. Brandt. *Data Analysis: Statistical and Computational Methods for Scientists and Engineers*. Springer, New York, 1999.
- [26] A Kankainen, J Äystö, and A Jokinen. High-accuracy mass spectrometry of fission products with penning traps. *J. Phys. G*, 39(9):093101, 2012.
- [27] G. Audi, A.H. Wapstra, and C. Thibault. The ame2003 atomic mass evaluation (ii). *Nucl. Phys A*, 729:337, 2003.
- [28] M.V. Stoitsov, N. Schunck, M. Kortelainen, N. Michel, H. Nam, E. Olsen, J. Sarich, and S. Wild. Axially deformed solution of the skyrme-hartreefockbogoliubov equations using the transformed harmonic oscillator basis (ii) hfbtho v2.00d: A new version of the program. *Comput. Phys. Commun.*, 184:1592, 2013.
- [29] B. Alex Brown. Neutron radii in nuclei and the neutron equation of state. *Phys. Rev. Lett.*, 85:5296, 2000.
- [30] R.J. Furnstahl. Neutron radii in mean-field models. *Nucl. Phys. A*, 706:85, 2002.
- [31] X. Roca-Maza, M. Centelles, X. Viñas, and M. Warda. Neutron skin of ^{208}Pb , nuclear symmetry energy, and the parity radius experiment. *Phys. Rev. Lett.*, 106:252501, 2011.
- [32] J. Piekarewicz, B. K. Agrawal, G. Colò, W. Nazarewicz, N. Paar, P.-G. Reinhard, X. Roca-Maza, and D. Vretenar. Electric dipole polarizability and the neutron skin. *Phys. Rev. C*, 85:041302, 2012.
- [33] P.-G. Reinhard and W. Nazarewicz. Information content of the low-energy electric dipole strength: Correlation analysis. *Phys. Rev. C*, 87:014324, 2013.
- [34] P.-G. Reinhard, J. Piekarewicz, W. Nazarewicz, B. K. Agrawal, N. Paar, and X. Roca-Maza. Information content of the weak-charge form factor. *Phys. Rev. C*, 88:034325, 2013.
- [35] W. Nazarewicz, P. G. Reinhard, W. Satuła, and Vretenar D. Symmetry energy in nuclear density functional theory. *Eur. Phys. J. A*, 50:20, 2014.
- [36] M. Warda, X. Viñas, X. Roca-Maza, and M. Centelles. Neutron skin thickness in the droplet model with surface width dependence: Indications of softness of the nuclear symmetry energy. *Phys. Rev. C*, 80:024316, 2009.
- [37] F. J. Fattoyev and J. Piekarewicz. Neutron skins and neutron stars. *Phys. Rev. C*, 86:015802, 2012.
- [38] De J.N. Agrawal, B.K. and S.K. Samaddar. Determining the density content of symmetry energy and neutron skin: An empirical approach. *Phys. Lett. B*, 572:152, 2003.
- [39] James M. Lattimer. The nuclear equation of state and neutron star masses. *Annu. Rev. Nucl. Part. Sci.*, 62:485, 2012.

- [40] Andrew W. Steiner, James M. Lattimer, and Edward F. Brown. The neutron star mass-radius relation and the equation of state of dense matter. *ApJ*, 765:L5, 2013.
- [41] S. Abrahamyan et al. Measurement of the neutron radius of ^{208}Pb through parity violation in electron scattering. *Phys. Rev. Lett.*, 108:112502, 2012.
- [42] C. J. Horowitz et al. *Phys. Rev. C*, 85:032501(R), 2012.
- [43] PREX-II Proposal to Jefferson Lab. <http://hallaweb.jlab.org/parity/prex/prexII.pdf>.
- [44] CREX Proposal to Jefferson Lab. http://hallaweb.jlab.org/parity/prex/c-rex2013_v7.pdf.
- [45] B. G. Carlsson, J. Dobaczewski, and M. Kortelainen. Local nuclear energy density functional at next-to-next-to-next-to-leading order. *Phys. Rev. C*, 78:044326, 2008.
- [46] F Raimondi, K Bennaceur, and J Dobaczewski. Nonlocal energy density functionals for low-energy nuclear structure. *J. Phys. G*, 41:055112, 2014.